SANDIA REPORT

Enclosure 1: #64

SAND87—0406
Internal Distribution Only
Printed March 1987

Thermal Analysis of the Anti-Submarine Penetrator Surface Pressure Transducers

Douglas N. Benton

Prepared by
Sandia National Laboratories
Albuquerque, New Mexico 87185 and Livermore, California 94550
for the United States Department of Energy
under Contract DE-AC04-76DP00789

DEPARTMENT OF ENERGY DECLASSIFICATION REVIEW
REVIEW AUTHORIZED BY: DOE 475.1b
REVIEWER (ADD): NAME: H A Schmitt
DATE: 3/13/08
DETERMINATION (CIRCLE NUMBER(S))
1. CLASSIFICATION RETAINED
2. CLASSIFICATION CHANGED TO:
3. CONTAINS NO DOE CLASSIFIED INFO
4. COORDINATE WITH:
5. CLASSIFICATION CANCELLED
6. CLASSIFIED INFO BRACKETED
7. OTHER (SPECIFY): Not responsive
Not reviewed

SF2900Q(8-81)

95SA20B000277

```
TTTTTTTTTT   66666666666666666666666666666666666666666666666666666666666666666666666666666666666666666666666666666666666666   TTTTTTTTTT
TTTTTTTTTT   66666666666666666666666  SANDIA NATIONAL LABORATORIES AERODYNAMICS VAX 8600  66666666666666666666666   TTTTTTTTTT
TTTTTTTTTT   66666666666666666666666666666666666666666666666666666666666666666666666666666666666666666666666666666666666666   TTTTTTTTTT

                                DDDD   N   N  BBBB   EEEEE  N   N  TTTTT   000
                                D   D  N   N  B   B  E      N   N    T    0   0
                                D   D  NN  N  B   B  E      NN  N    T    0   0
                                D   D  N N N  BBBB   EEEE   N N N    T    0   0
                                D   D  N  NN  B   B  E      N  NN    T    0   0
                                D   D  N   N  B   B  E      N   N    T    0   0
                                DDDD   N   N  BBBB   EEEEE  N   N    T     000

                                  AAAAAA      SSSSSSSS  PPPPPPPP
                                  AAAAAA      SSSSSSSS  PPPPPPPP
                                AA      AA  SS          PP      PP
                                AA      AA  SS          PP      PP
                                AA      AA  SS          PP      PP
                                AA      AA  SS          PP      PP
                                AA      AA    SSSSSS    PPPPPPPP
                                AA      AA    SSSSSS    PPPPPPPP
                                AAAAAAAAAA          SS  PP
                                AAAAAAAAAA          SS  PP
                                AA      AA          SS  PP
                                AA      AA          SS  PP
                                AA      AA  SSSSSSSS    PP
                                AA      AA  SSSSSSSS    PP

                                BBBBBBBB      IIIIII    TTTTTTTTTT      ;;;;        11
                                BBBBBBBB      IIIIII    TTTTTTTTTT      ;;;;        11
                                BB      BB      II          TT          ;;;;      1111
                                BB      BB      II          TT          ;;;;      1111
                                BB      BB      II          TT                      11
                                BB      BB      II          TT                      11
                                BBBBBBBB        II          TT          ;;;;        11
                                BBBBBBBB        II          TT          ;;;;        11
                                BB      BB      II          TT          ;;;;        11
                                BB      BB      II          TT          ;;;;        11
                          ....  BB      BB      II          TT            ;;        11
                          ....  BB      BB      II          TT            ;;        11
                          ....  BBBBBBBB      IIIIII        TT          ;;      111111
                          ....  BBBBBBBB      IIIIII        TT          ;;      111111


File  $7$DUA3:[DNBENTO.ASP.PRESS]ASP.BIT;1 (5287,9,0), last revised on  4-MAR-1987 08:52, is a 375 block sequential file owned by
UIC [176,1].  The records are variable length with implied (CR) carriage control.  The longest record is 78 bytes.

Job BOX.034 (1572) queued to SAV07_LCB0 on 4-MAR-1987 08:52 by user DNBENTO, UIC [176,1], under account 0560300 at priority 4,
started on printer _SAV07$LCB0: on 4-MAR-1987 08:52 from queue SAV07_LCB0.

TTTTTTTTTT   66666666666666666666666666666666666666666666666666666666666666666666666666666666666666666666666666666666666666   TTTTTTTTTT
TTTTTTTTTT   66666666666666666666666  Digital Equipment Corporation - VAX/VMS Version V4.3  66666666666666666666666   TTTTTTTTTT
TTTTTTTTTT   66666666666666666666666666666666666666666666666666666666666666666666666666666666666666666666666666666666666666   TTTTTTTTTT
```

SAND87-0406
Internal Distribution Only
Printed March 1987

Thermal Analysis of the Anti-Submarine Penetrator Surface Pressure Transducers

Douglas N. Benton
Aerothermodynamics Division
Sandia National Laboratories
Albuquerque, NM 87185

Abstract

Analysis of the Anti-Submarine Penetrator aerothermodynamic environment showed that the surface pressure transducers mounted in the vehicle case required thermal protection. Recessing the transducers below the case surface and covering them with a 0.050-in. layer of RTV compound provided sufficient thermal protection but reduced transducer frequency response and repeatability. Mounting the transducers at the bottom of open cavities below the vehicle surface also proved unacceptable. The large cavity depth to cavity diameter ratio required to sufficiently lower heat transfer to the tranducer, a value of about 26, unacceptably reduced transducer frequency response. The final solution consisted of filling the open cavity, having a depth of 0.070 in. and a diameter of 0.050 in., with a viscous silicone oil. The incompressible silicone oil does not significantly affect frequency response and insulates the transducer from the freestream environment.

Acknowledgments

The author acknowledges the contributions of several people. L. R. Rollstin (1555) supplied the ASP vehicle atmospheric trajectory. M. T. Ferrario (8152) supplied construction details of the ASP vehicle which were necessary to the analysis. S. McAlees (1553) suggested recessing the transducers below the surface in cavities, which was part of the final solution. W. L. Oberkampf (1556) provided the vehicle's trajectory after water entry, suggested the final solution to the pressure transducer thermal protection problem, and held overall responsibility for specification of the ASP surface pressure instrumentation.

Contents

1 Introduction 8

2 ASP Vehicle Description 8

3 Vehicle Trajectory 9

4 Pressure Instrumentation 10

5 Aerodynamic Heating Analysis 11

6 Indepth Conduction Analysis 11
- 6.1 Vehicle Case Conduction Analysis 13
- 6.2 Pressure Transducer Conduction Analysis 15
- 6.3 Subsurface Cavity Mounted Transducers 17
- 6.4 Silicone Oil Filled Cavity 18
- 6.5 Transducer Sensitivity to Transverse Temperature Gradients 18

7 Heat Transfer to the Bottom of a Cavity 21

8 Conclusion 24

9 References 25

A Vehicle Trajectory 26
- A.1 Computed Atmospheric Trajectory 27
- A.2 Trajectory After Water Entry 29

B Gap Heating Data Derived From Reference 11 30

List of Figures

1 ASP Vehicle 8

2 ASP Atmospheric Trajectory 9

3 ASP Trajectory After Water Entry 10

4 Computed ASP Heat Transfer Rates 12

5 Computed ASP Heat Transfer Rates at the 27.33-in. Station After Water Entry 13

6 Predicted ASP Case Temperatures at the 27.33-in. Station 14

7 Predicted ASP Case Temperatures at the 27.33-in. Station After Water Entry 15

8 Thermal Model and Predicted Pressure Transducer Temperature for the Transducer Mounted Flush With the Vehicle Surface 16
9 Cavity Mounted Pressure Transducer Configuration 17
10 Nestler, Saydah, and Auxer Gap Bottom Heating Correlation Plotted for End of Trajectory Conditions at the 27.33-in. Station 18
11 Thermal Model and Predicted Pressure Transducer Temperature Beneath a Cavity Filled with Silicone Oil 19
12 Thermal Model and Predicted Pressure Transducer Temperature Beneath a Duroid Washer 20
13 Nestler, Saydah, and Auxer Gap Bottom Heating Correlation 24

Nomenclature

H	cavity depth
k_d	thermal conductivity of air along the cavity dividing streamline
k_s	thermal conductivity of air at the vehicle surface
L	cavity diameter or length
M_e	boundary layer edge Mach number
q	compressible heat flux to flat plate
q_b	heat flux to the bottom of a cavity
q_c	heat flux crossing the dividing streamline into a cavity
q_i	incompressible heat flux to a flat plate
q_s	heat flux to the surface if the cavity were not present
Re_s	Reynolds number based on surface streamlength from the vehicle nosetip and boundary layer edge properties
T	temperature (deg R)
u_d	velocity along the cavity dividing streamline

Greek Symbols

δ	boundary layer thickness
δ^*	boundary layer displacement thickness
μ_d	viscosity of air along the dividing streamline
Φ	variable defined by Equation 3
σ	turbulent shear layer spread parameter

1 Introduction

The purpose of the Anti-Submarine Penetrator (ASP) Program is to develop a weapon capable of Arctic ice penetration or water entry without broaching. The test program for the RAP-200 series vehicle includes three instrumented flights from Kauai with a water entry. The instrumentation for these flights includes eight transducers which measure surface pressures after the water entry. The relatively low aerothermodynamic heating experienced by the vehicle poses no threat to the structural integrity of the vehicle. The pressure transducers, however, are only temperature compensated over a maximum range of 250 deg R. Since the water at depth is at a temperature of 520 deg R, the transducer temperature can not exceed 770 deg R without exceeding the compensation range. At the point in the trajectory where the vehicle reaches an altitude of 5177 ft and a Mach number of 2.37 the boundary layer recovery temperature is 973 deg R. Because of their low thermal capacity and isolation from the vehicle case, the temperature of pressure transducers mounted flush with the vehicle surface will be close to the boundary layer recovery temperature. This report discusses the analysis of the transducer aerothermal environment and the design of a thermal protection system to insulate the transducers from excessive heating.

2 ASP Vehicle Description

Figure 1 shows the ASP external configuration. The vehicle is a 64.92-in. long tangent ogive-cone with a 14.7-in. diameter base. The 20-caliber, 294-in. radius, ogive forebody is 32.32 in. long and begins with an approximately 0.10-in. radius spherical nose. At the 32.32-in. station, where the body diameter is 9.25 in., the ogive is tangent to a 4.78-degree half-angle conical frustum. The vehicle case is 0.25-in. thick 4340 steel and the forebody contains a tungsten alloy ballast. Overall weight of the vehicle is 770 lbs.

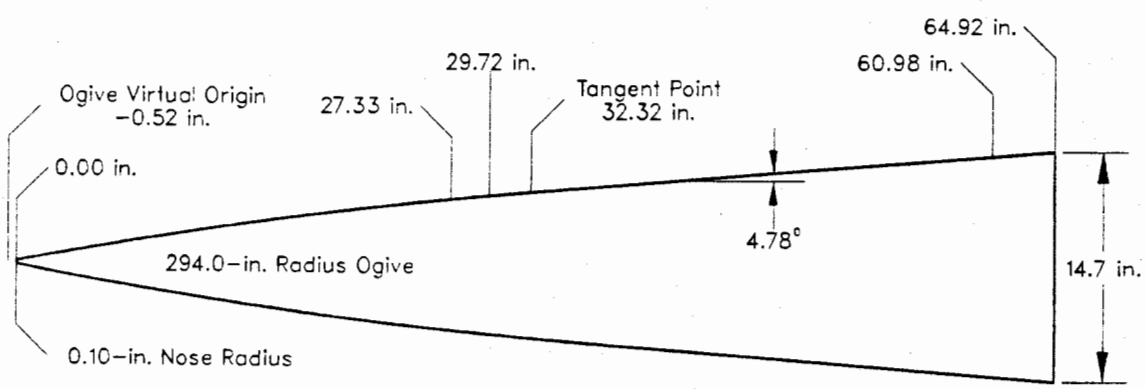

Figure 1: ASP Vehicle

3 Vehicle Trajectory

The ASP trajectory contains both an atmospheric portion and an underwater portion following water entry. Although the only significant heating occurs in the atmosphere, the underwater portion of the trajectory is included in the thermal analysis to estimate the rate at which the vehicle cools after water entry. Appendix A contains a listing of the computed atmospheric trajectory and the trajectory after water entry.

Figure 2 shows the atmospheric trajectory used for the heating analysis. The trajectory consists of powered flight for the first 3.5 seconds to a Mach number of 1.61 and an altitude of 1448 ft, followed by a ballistic cruise to an apogee at Mach 0.89 and an altitude of 6851 ft at 20.3 seconds. At 26.7 seconds into the flight, at Mach 0.85 and an altitude of 6200 ft, the second stage rocket burns for 2 seconds and accelerates the vehicle to Mach 2.37 at an altitude of 5177 ft. The final plunge into the water occurs at 36.7 seconds and a Mach number of 1.8.

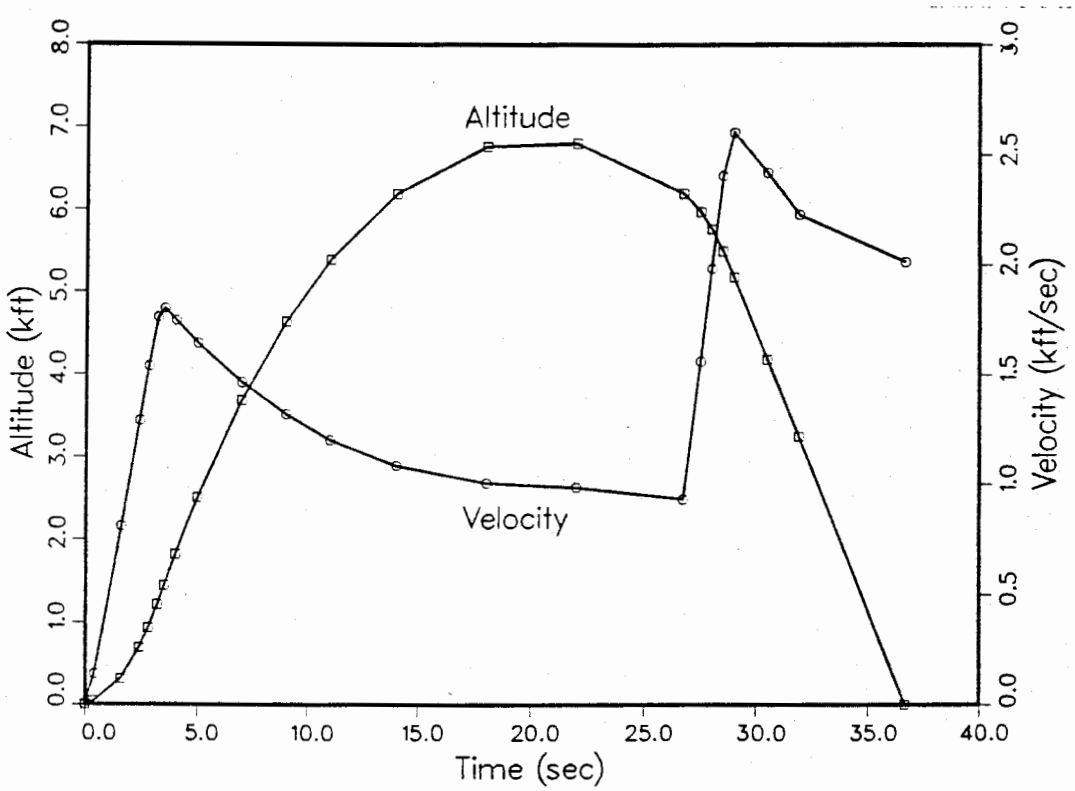

Figure 2: ASP Atmospheric Trajectory

Figure 3 shows the underwater trajectory of the vehicle after water entry at 2012 ft/sec. This trajectory represents a worst case scenario in that the vehicle's maximum water entry velocity is approximately 2000 ft/sec. After 1 second the vehicle has slowed to 105 ft/sec and reached a depth of 243 ft. After 6.8 seconds the vehicle has slowed to 45 ft/sec and reached the recovery system deployment depth of 500 ft. The water temperature varied from 542 deg R at the surface to 531 deg R at a depth of 500 ft.

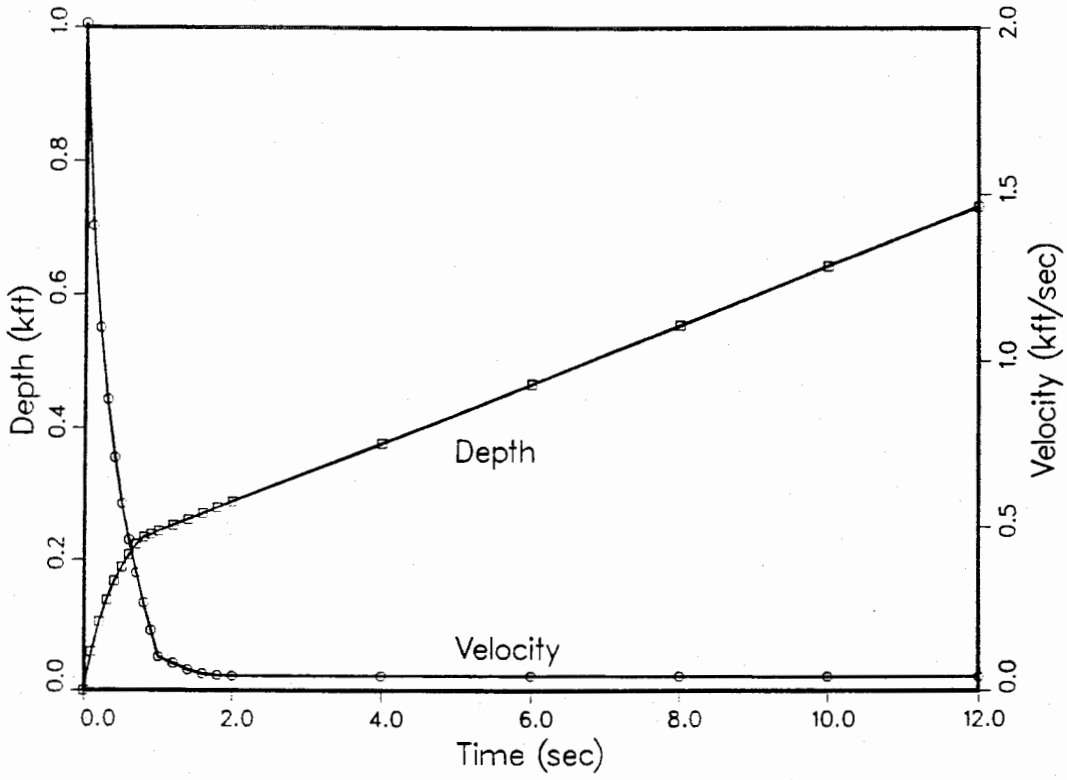

Figure 3: ASP Trajectory After Water Entry

4 Pressure Instrumentation

Transducer locations are measured along the vehicle axis from the nosetip. One pressure transducer is mounted at each of the axial locations 27.33 in. and 29.72 in. Four pressure transducers are mounted 60.98 in. from the vehicle nosetip. The remaining two transducers are mounted on the base of the vehicle. The transducer located at 27.33 in., where the surface pressure coefficient is unity when the vehicle is submerged, measures water depth pressure to obtain an independent depth measurement. The other seven transducers measure the low pressures existing in the cavities formed on the vehicle surface immediately after water entry. These cavities collapse quickly and the pressure transducer readings will then go off scale.

The pressure transducer assembly is 0.140 in. in diameter and 0.155 in. long. The sensing element of the depth pressure transducer consists of a thin silicon wafer 0.0017 in. thick. The other transducer sensing elements are 0.00045 in. thick silicon wafers. The sensing elements of all the transducers are covered by 0.010 in. of RTV topped with a 0.005-in. stainless steel screen exposed to the freestream pressure. Properties of RTV used in this analysis are those of Dow Corning 3145. The screen is assumed to have 50% porosity with the pores in the screen filled with RTV. Filling the screen pores with RTV eliminates the possibility of roughness augmented heating. The thermal properties of the screen are taken as the average of those of RTV and 304 stainless steel.

5 Aerodynamic Heating Analysis

The LOVEL low velocity aeroheating program [10] was used to predict the heating environment experienced by the vehicle. This program is useful for predicting heat transfer rates on vehicles at Mach numbers less than 6. The code predicts heating on simple shapes such as flat plates, sharp cones and sharp wedges, and sphere-cones and cylinder-wedges. It makes use of empirical heat transfer correlations, based on the distance from the vehicle nosetip, to calculate coldwall heat transfer rates. The coldwall heat transfer rate is referenced to an arbitrary wall temperature of 536 deg R.

To calculate the ASP aerodynamic heating, the vehicle was treated as two distinct sphere-cones. A tangent line to the ASP surface at the 27.33-in. station forms an angle of 5.7 degrees with the vehicle centerline. The forward section, therefore, was treated as a sphere-cone with body half-angle of 5.7 degrees. The rear station was treated as a sphere-cone with body half-angle of 4.7 degrees. Heat transfer calculations were made at the 27.33-in. and the 60.98-in. stations. Heating at the 29.72-in. station will be slightly less than heating at the 27.33-in. station. Turbulent flow was assumed for all of the calculations. The Reynolds number, based on streamwise distance from the nosetip and boundary layer edge properties, at the 27.33-in. station and the end of the vehicle trajectory is 30 million, well within the regime where turbulent flow is expected.

Figures 4 shows the predicted coldwall heat transfer rates at the vehicle nosetip, 27.33-in. station, and 60.98-in. station. The heating is highest at the nosetip and decreases as distance from the nosetip increases. Experimental results show that reentry vehicle base heating in hypersonic flow is an order of magnitude lower than side wall heating [4]. Although these results can not be extrapolated to the low supersonic Mach numbers of the ASP experiment, the base should see significantly lower heat transfer rates than the vehicle side wall.

To calculate the rate at which the vehicle cools upon entering the water, the NEPTUNE program was written using the sharp cone heat transfer relationships employed by LOVEL but with water properties. The program took advantage of the fact that at the 27.33-in. station the boundary layer edge pressure is the same as the freestream pressure after water entry. The boundary layer edge velocity, therefore, is the same as the freestream velocity. Figure 5 shows a plot of the coldwall heat transfer rate for the underwater portion of the trajectory at the 27.33-in. station.

6 Indepth Conduction Analysis

All of the conduction analysis was performed on one-dimensional models even when the nature of the problem justified a two-dimensional model. The one-dimensional solution always bracketed the effects of interest. The Charring Material Ablation (CMA) computer program [3] was used with heating input from LOVEL and NEPTUNE to calculate a one-dimensional indepth conduction solution. The CMA program uses a surface energy balance to couple the coldwall convective heat transfer prediction to the

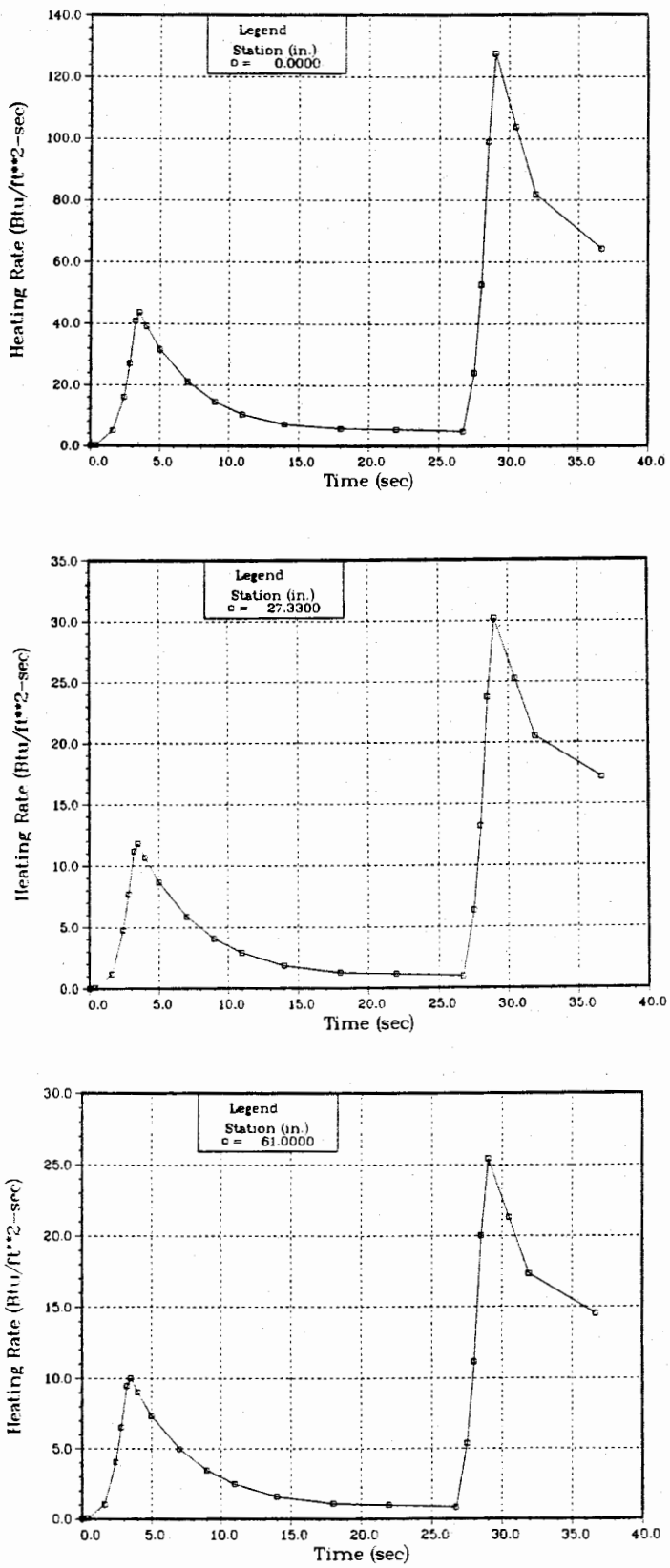

Figure 4: Computed ASP Heat Transfer Rates

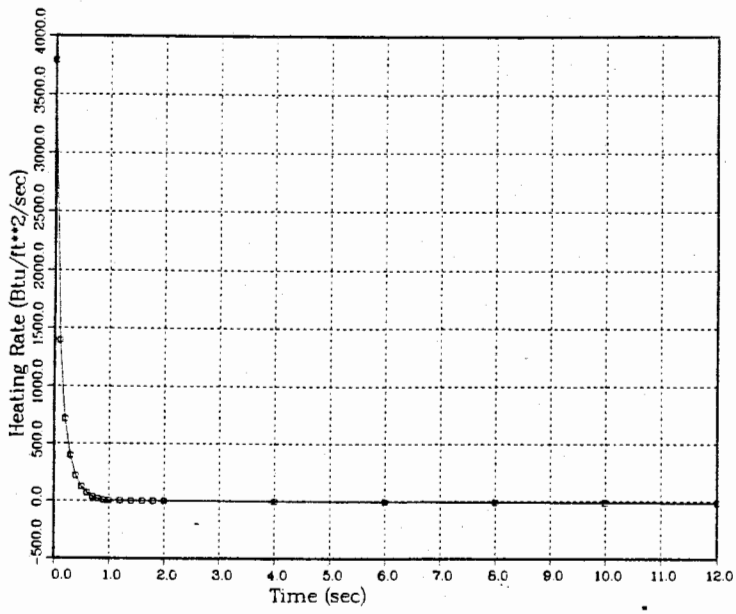

Figure 5: Computed ASP Heat Transfer Rates at the 27.33-in. Station After Water Entry

conduction solution. The program empirically corrects the input coldwall convective heat transfer coefficient to account for the calculated wall temperature deviation from the coldwall datum of 536 deg R.

6.1 Vehicle Case Conduction Analysis

To evaluate the thermal environment surrounding a pressure transducer mounted in the vehicle case, surface and indepth temperatures were predicted at the 27.33-in. station. Uncertainty in the construction details of the vehicle required that the analysis be performed for two geometries. The first geometry consisted of the case separated from the ballast by an 0.015-in. air filled gap. The thermal resistance of the gap , 285 $ft^2 * sec * R/Btu$, effectively isolates the case from the ballast. The analysis of the first geometry, therefore, used an insulated case back-wall boundary conditiion. The second geometry accounted for the heat sink provided by the tungsten alloy ballast by assuming that the gap between the case and ballast was filled with RTV. Filling the gap with RTV yields a gap thermal resistance of 46 $ft^2 * sec * R/Btu$ and allows for some thermal communication between the case and the ballast. Figure 6 shows predicted in-depth temperatures for both cases. The surface temperature reached maximums of 700 deg R and 685 deg R for the first and second geometries, respectively. Temperatures at the backface of the case were 689 deg R and 669 deg R, respectively.

Figure 7 shows the temperatures produced by the CMA program with surface heating input from the NEPTUNE program. The case was in thermal communication with the ballast with 0.015 in. of RTV placed between the case and ballast. For these calculations the hotwall temperature correction in CMA, developed for air, was disabled

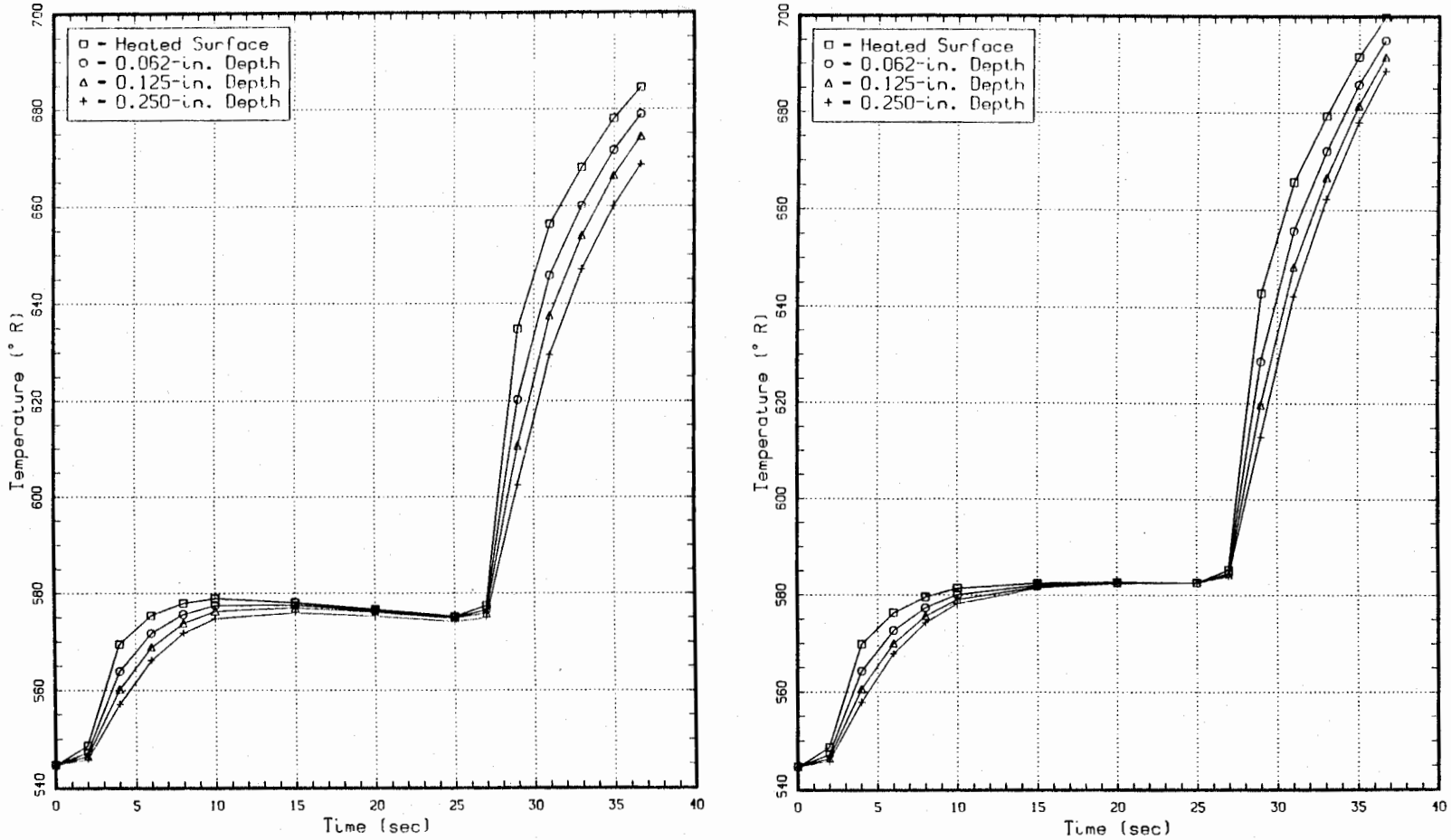

Figure 6: Predicted ASP Case Temperatures at the 27.33-in. Station

and no correction was made to the coldwall heat transfer coefficient calculated by NEPTUNE. Calculations made with the CMA program showed that the case surface cooled to within 8 deg R of the water temperature 1 second after water entry. After 2 seconds in the water the case surface temperature reached an asymptote of 4 deg R above the water temperature.

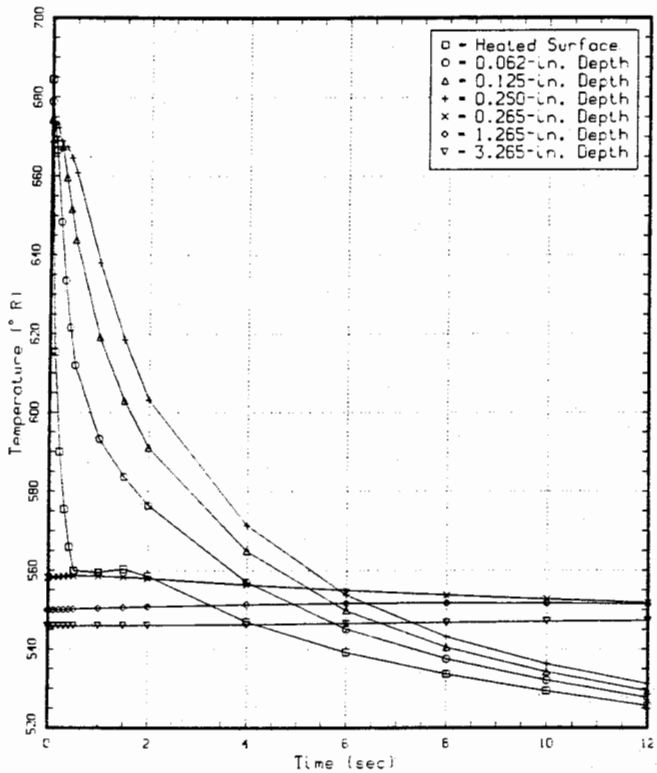

Figure 7: Predicted ASP Case Temperatures at the 27.33-in. Station After Water Entry

6.2 Pressure Transducer Conduction Analysis

Because the pressure transducers have a much lower thermal capacity than the vehicle case and are thermally isolated from the case, they reach higher temperatures than the case. Original plans called for pressure transducers mounted flush with the vehicle surface. Figure 8 shows the thermal model used in the conduction calculations and the predicted in-depth temperatures at the 27.33-in. station for this mounting configuration. The silicon temperature reaches 915 deg R, well above the maximum acceptable temperature. The 0.005 in. thick screen and 0.010 in. of RTV provide only minimal protection from the boundary layer recovery temperature. Recessing the transducer below the surface and adding additional layers of RTV would increase the thermal protection afforded the transducer but not without causing additional problems. A 0.050 in. thick layer of RTV lowers the maximum transducer temperature to 705 deg R, but also sacrifices transducer frequency response and repeatability.

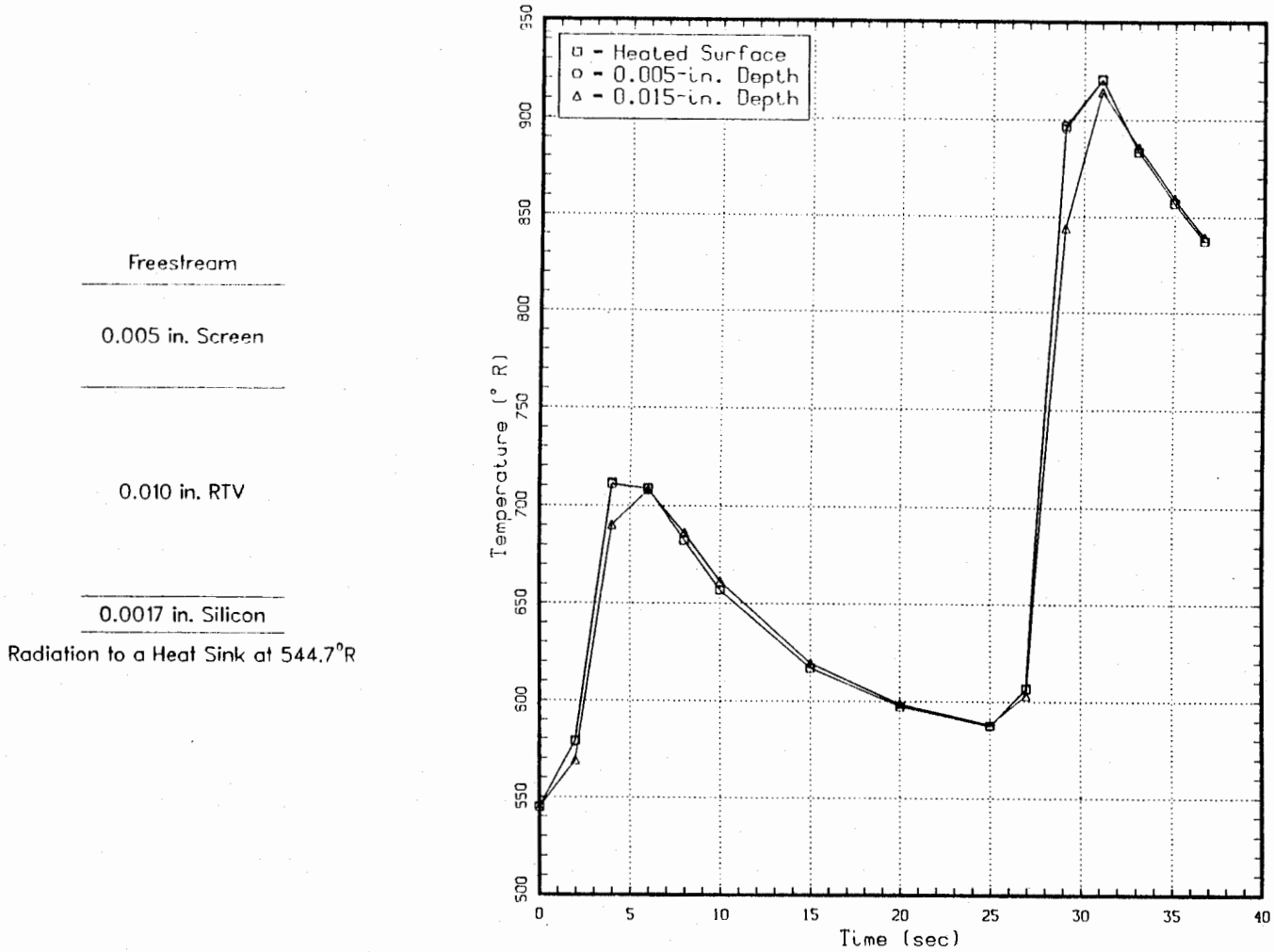

Figure 8: Thermal Model and Predicted Pressure Transducer Temperature for the Transducer Mounted Flush With the Vehicle Surface

6.3 Subsurface Cavity Mounted Transducers

To shield the transducers from the freestream environment, mounting the transducers in cavities below the vehicle surface, as shown in Figure 9, was investigated. An analysis with CMA showed that the heat transfer rate to the pressure transducer, q_b, must be lowered by a factor of 20 relative to the heat transfer rate to a pressure transducer mounted on the vehicle surface at the same position, q_s. Because the 0.25-in. case thickness limits the cavity depth to 0.070 in., the problem became one of choosing the cavity diameter to insure a low heat transfer rate at the cavity bottom. The minimum ASP transducer cavity diameter is 0.050 in. Smaller diameters yield a cavity diameter to depth ratio, L/H, small enough to significantly attenuate the transducer frequency response.

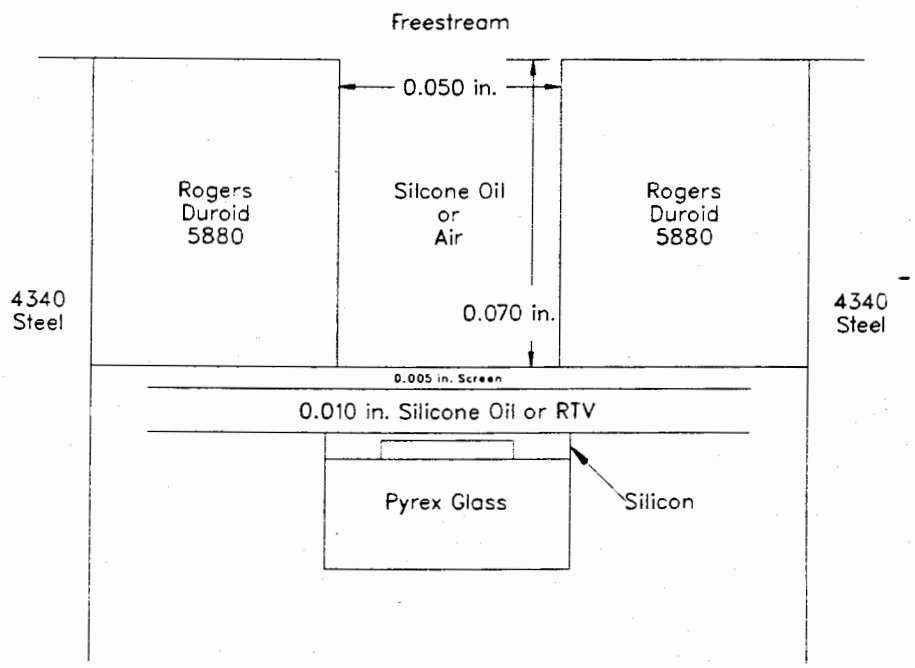

Figure 9: Cavity Mounted Pressure Transducer Configuration

Figure 10 shows q_b/q_s from a correlation developed by Nestler, Saydah, and Auxer [8] plotted versus H/L for conditions in the ASP vehicle boundary layer at the end of the air trajectory at the 27.33-in. station. Heat transfer to the bottom of cavities and the correlation plotted in Figure 10, are discussed more thoroughly later. Assuming that the correlation holds, Figure 10 shows that H/L = 26 is required to obtain $q_b/q_s = 0.05$. The maximum cavity depth of 0.070 in. and minimum cavity diameter of 0.050 in., or H/L = 1.4, yields $q_b/q_s = 0.68$. Transducer cavity depth limitations prevent use of this technique to protect the pressure transducers.

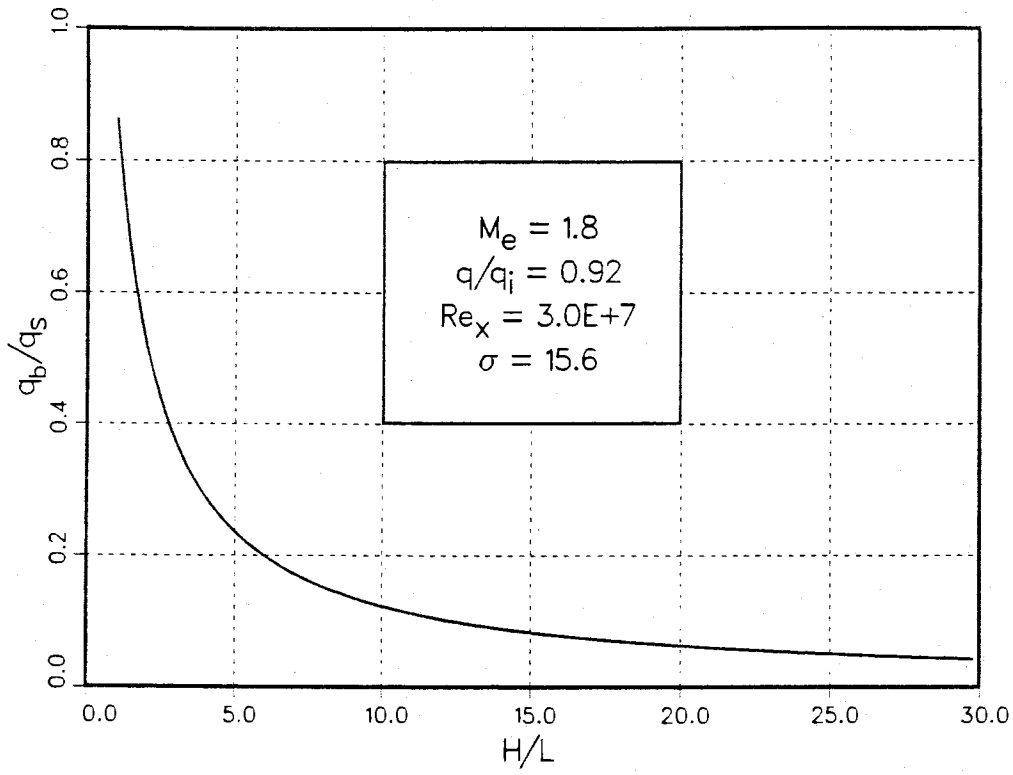

Figure 10: Nestler, Saydah, and Auxer Gap Bottom Heating Correlation Plotted for End of Trajectory Conditions at the 27.33-in. Station

6.4 Silicone Oil Filled Cavity

To overcome the limitations on the transducer cavity depth, the cavity will be filled with a viscous, essentially incompressible, silicone oil. This technique thermally insulates the pressure transducer and prevents any frequency response loss caused by the cavity. Because silicone oil causes RTV swelling, no RTV can be used in the transducer assembly. Therefore, the 0.010 in. of RTV seen in Figure 9 is replaced by silicone oil. Figure 11 shows the thermal model of the pressure transducer mounted below 0.071 in. of silicone oil and the results of the CMA conduction calculations. The transducer sees a maximum temperature of 636 deg R, well within the acceptable temperature range.

6.5 Transducer Sensitivity to Transverse Temperature Gradients

In addition to an absolute temperature sensitivity, the transducers also exhibit a sensitivity to transverse temperature gradients. To evaluate the magnitude of this effect, two one-dimensional temperature distributions are compared. Figure 12 shows the thermal model and temperature distribution through the Rogers Duroid 5880 insulator and the transducer assembly. The silicon wafer reaches a temperature of 587 deg R

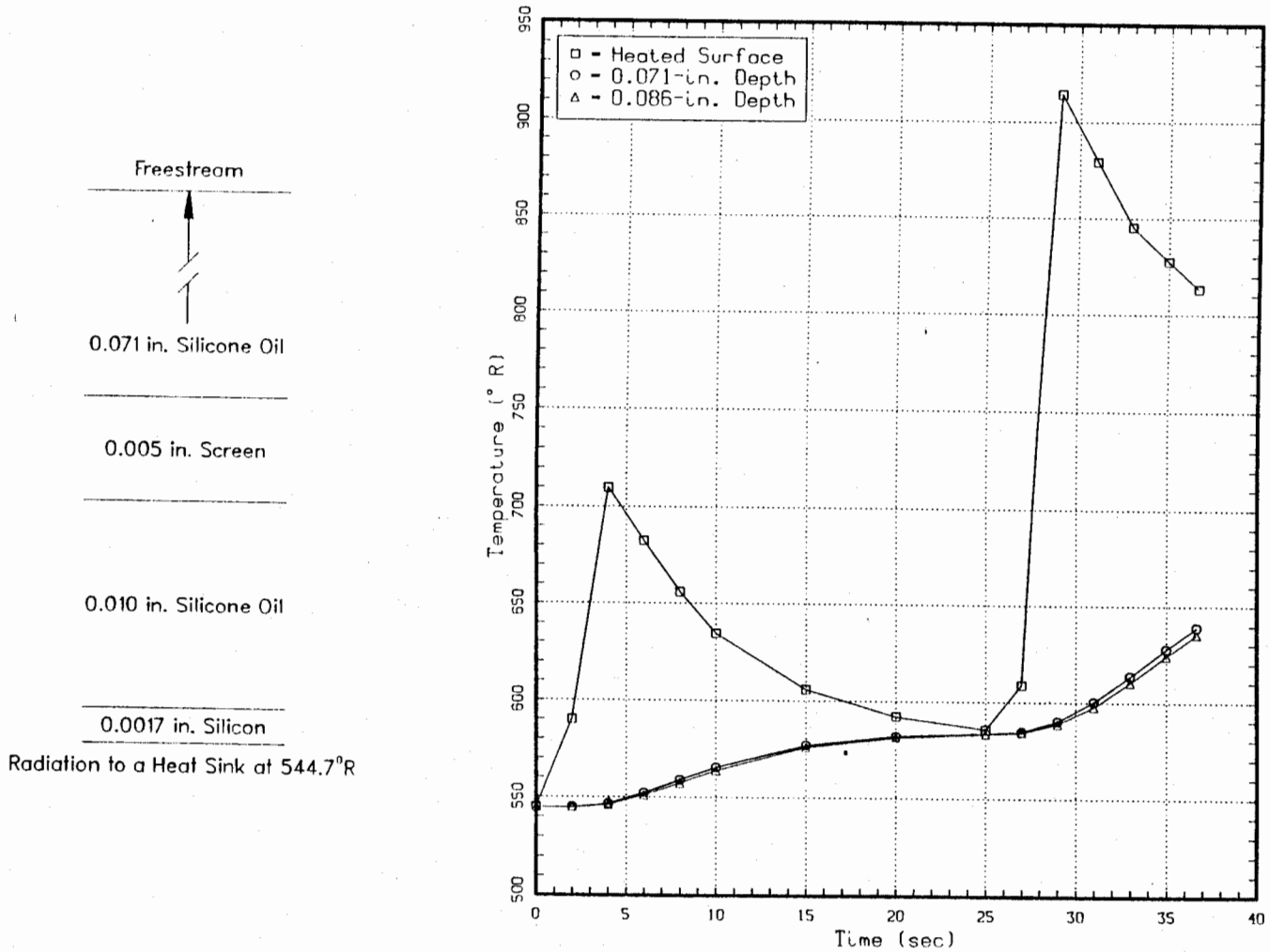

Figure 11: Thermal Model and Predicted Pressure Transducer Temperature Beneath a Cavity Filled with Silicone Oil

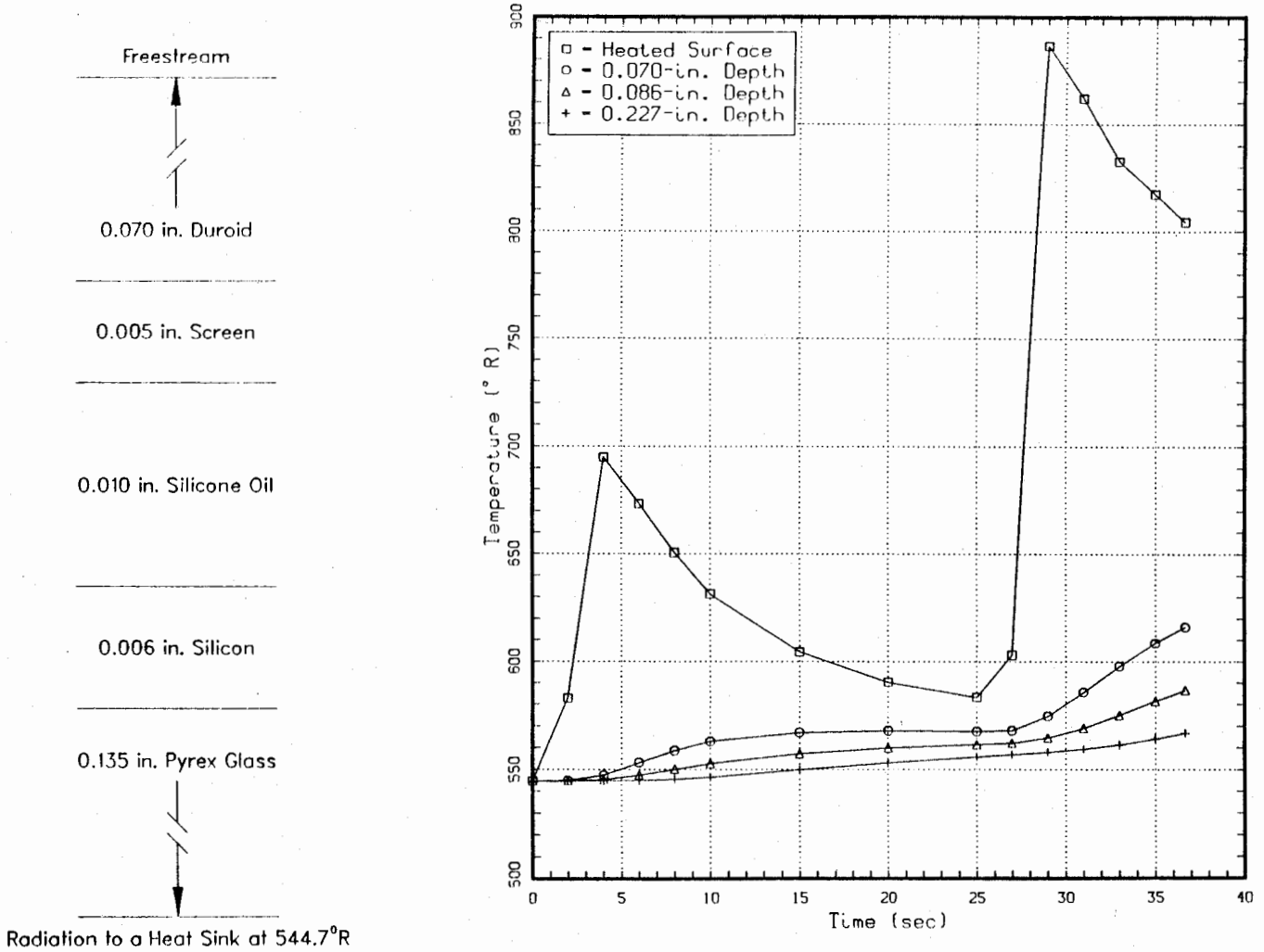

Figure 12: Thermal Model and Predicted Pressure Transducer Temperature Beneath a Duroid Washer

beneath the insulating washer. As shown earlier in Figure 11 , the silicon wafer reaches a temperature of 636 deg R beneath the cavity filled with silicone oil. The difference between these temperatures sets an upper bound of 49 deg R on the temperature difference between the center of the silicon wafer and the edge of the wafer. In reality, two-dimensional heat transfer effects will reduce this difference.

7 Heat Transfer to the Bottom of a Cavity

Very few experimental measurements of heat transfer to the bottom of a cavity and only crude theoretical analyses of the problem exist. The heat transfer to the bottom of a cavity depends on the state of the boundary layer, either laminar or turbulent, the cavity length in the flow direction, L, the cavity depth, H, boundary layer edge conditions, and any interaction between these variables. In addition, most previous research concentrated on understanding and quantifying the increase in heat transfer rates caused by reattachment of a cavity free shear layer rather than the attenuation of heat transfer at the bottom of a cavity. References [1,2,7] review the available literature on heat transfer in separated flows. Most investigators studied two-dimensional channels or rectangular notches. In order to estimate the cavity size needed to protect the ASP pressure tranducers, two-dimensional results are used to estimate the heat transfer at the bottom of a round hole. In [5], Nestler justified a two-dimensional analysis of measurements taken in round holes as representative of a slice through the middle of the holes.

The literature makes the distinction between a cavity and a gap. A cavity is large in the flow direction relative to the boundary layer thickness of the external flow. The ratio of cavity length to boundary layer thickness, L/δ, is much greater than 1. This feature allows simpler experimental setups because the apparatus can be of reasonable size. On the other hand, a gap has a value of L/δ less than or equal to 1. Not only does this complicate any theoretical analysis, it also means that the dimensions of any experimental investigation must be small and measurement uncertainty large. As noted before, the minimum ASP cavity diameter is 0.050 in. The GE reentry vehicle heating program [9] predicts a turbulent boundary layer thickness of 0.164 in. at the 27.33-in. station for a freestream Mach number of 1.8 and an altitude of 0.0 ft. This yields a L/δ ratio of 0.30. The ASP cavity, therefore, falls in the gap regime.

Most theoretical analyses or correlations of heat transfer to cavities and gaps, under either laminar or turbulent boundary layers, begin with calculation of the heat addition to the recirculating region. The heat addition is given by:

$$q_c = \frac{1}{L}\int_0^L \left[k_d \frac{\partial T}{\partial y} + u_d\,\mu_d \frac{\partial u}{\partial y}\right] dx \tag{1}$$

where

$k_d =$ thermal conductivity of air along the dividing streamline

$\frac{\partial T}{\partial y}$ = temperature gradient normal to the dividing streamline

u_d = velocity along the dividing streamline

μ_d = viscosity of air along the dividing streamline

$\frac{\partial u}{\partial y}$ = velocity gradient normal to the dividing streamline

The first term represents the heat flux across the streamline dividing the flow between the recirculating region and the external flow. The second term represents the energy addition through viscous shear work. For a cavity under a turbulent boundary layer, the assumption that an asymptotic turbulent free shear layer originates at the upstream cavity wall yields a simplified theoretical analysis for the heat addition to the recirculating region, [6]. The initial non-asymptotic growth is accounted for by a simple coordinate shift. This form of analysis will not work for gaps under turbulent boundary layers because the free shear layer does not come close to asymptotic behaviour over the short gap length. For a cavity or gap beneath a laminar boundary layer the free shear layer development is based on Blasius initial profiles. After the heat addition to the cavity is found, some distribution along the cavity walls is assumed. For example, in Reference [6] Nestler asssumed that the heat flux distribution in the recirculating region corresponded to a wall jet heat flux decay. Finally, most data for heat transfer to cavities is presented as the ratio of heat flux to the bottom of the cavity divided by the heat flux to the surface if the cavity were not present, q_b/q_s. The heat flux to the surface is given by:

$$q_s = k_s \frac{\partial T}{\partial y} \tag{2}$$

where

k_s = thermal conductivity of the air at the vehicle surface

$\frac{\partial T}{\partial y}$ = temperature gradient normal to the vehicle surface

Note that as the cavity width goes to zero, the heat addition to the cavity, Equation 1, becomes the same as the heat transfer to the surface if the cavity were not present, Equation 2.

Only two papers of use in this problem were found. In Reference [11], Weinstein, Avery, and Chapman studied heating to the gaps and surfaces of reusable surface insulation tile arrays beneath a turbulent boundary layer. Their goal was to simulate the aerodynamic heating problems expected on the shuttle orbiter during Earth reentry. The investigators varied displacement thickness and gap width. The displacement thickness was varied by changing the angle of attack of the flat plate in which the array was mounted. This changed the local Mach number and other boundary layer edge conditions. The freestream conditions in the tunnel remained constant. The investigators did not actually measure heat fluxes at the bottom of gaps between insulation tiles, but measured heat fluxes along the sides of the gaps. For this study it was assumed that

the measured heat flux ratios on the upstream and downstream sides of the gaps at a given depth could be averaged to obtain the equivalent heat flux ratio to the bottom of a gap with the same depth. Appendix B contains the data points obtained in this manner.

In Reference [8], Nestler, Saydah, and Auxer measured the heat transfer along the walls and bottoms of cavities and gaps under a turbulent boundary layer. They also developed a correlation of the heat transfer to the bottom of both cavities and gaps using the data presented in the paper and other experimental data.

$$\frac{q_b}{q_s} = 1.88 \frac{Re_s^{0.2}}{\left(1 + 2\frac{H}{L}\right)\left(1 + \frac{\gamma-1}{2}M_e^2\right)\frac{q}{q_i}\sigma} = 1.88\,\Phi \tag{3}$$

where

$Re_s =$ Reynolds number based on boundary layer edge conditions and distance from the leading edge of the flat plate.

$M_e =$ boundary layer edge Mach number

$\frac{q}{q_i} =$ ratio of compressible to incompressible heat flux on a flat plate

$\sigma =$ turbulent shear layer spread parameter, assumed to vary linearly from a value of 12 at M = 0, to 16 at M = 2 and constant thereafter, [6].

Nestler et al. developed the correlation by deriving a relationship for q_c/q_s assuming the growth of an asymptotic turbulent free shear layer over the cavity. That analysis produced

$$\frac{q_c}{q_s} \approx \frac{Re_s^{0.2}}{\left(1 + \frac{\gamma-1}{2}M_e^2\right)\frac{q}{q_i}\sigma} \tag{4}$$

They then assumed that the heat flux to the bottom of the recirculating region is proportional to the average heat flux to the walls of the recirculating region.

$$q_b \approx q_c \frac{L}{L + 2H} = q_c \frac{1}{1 + 2\frac{H}{L}} \tag{5}$$

Note that the development of the correlation does not apply to gaps because of the assumption of an asymptotic turbulent free layer growing over the cavity. Note also that the cavity or gap length has no effect on the q_c/q_s ratio. As mentioned before, q_c/q_s should go to 1 as the recirculating region length goes to 0.

Figure 13 shows the correlation plotted with the two experimental gap data points from Reference [8] and four points derived from Reference [11]. In Reference [11], Weinstein et al. did not give sufficient information to allow calculation of the boundary layer edge conditions when the flat plate model was positioned at an angle of attack. The four points plotted in Figure 13 correspond to the 0.0 degree angle of attack condition. The figure shows that the correlation, developed for cavities, does not do well in the gap regime. The correlation does, however, split the data.

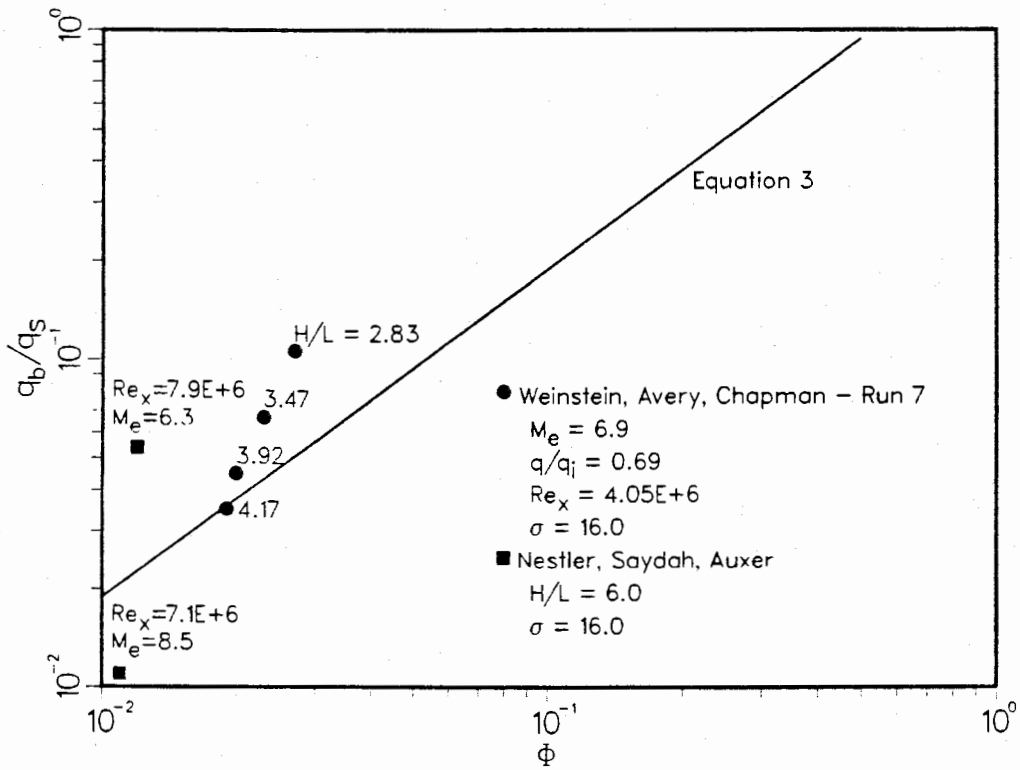

Figure 13: Nestler, Saydah, and Auxer Gap Bottom Heating Correlation

8 Conclusion

Although the aerothermal environment experienced by the ASP vehicle is mild by comparison with reentry vehicle environments, the fragile construction of the surface pressure transducers nevertheless required that they be insulated from that environment. A proposal to cover the transducers with RTV proved unacceptable because the required thick layer of RTV destroyed transducer frequency response and repeatability. Recessing the transducer below the surface also failed to provide a solution to the thermal protection problem because the required cavity depth to diameter ratio would again destroy transducer frequency response. The solution to the problem was found by recessing the pressure transducer below the surface in a shallow cavity and filling the cavity with a viscous, incompressible, silicone oil.

9 References

[1] A. F. Charwat, *Supersonic Flows with Embedded Shock Regions*, Advances in Heat Transfer, Academic Press, 1970.

[2] L. S. Fletcher, D. G. Briggs, and R. H. Page, *Heat Transfer in Separated and Reattached Flows*, Israel Journal of Technology, vol. 12, 1974, pp. 236-261.

[3] L. M. Lauger, P. C. Kaestner, and B. F. Blackwell, *Operation Instructions for Charring Material Ablation Code*, SLA-73-0745, Sandia National Laboratories, Albuquerque, August, 1973, revised by S. G. Beard, December 1985.

[4] S. McAlees, private communication, Aerothermodynamics Division 1553, Sandia National Laboratories, January, 1986.

[5] D. E. Nestler, *Hypersonic Laminar Cavity Heat Transfer*, Proceedings of the 4th International Heat Transfer Conference, vol. 3, Versailles, September, 1970.

[6] D. E. Nestler, *An Engineering Analysis of Reattaching Shear Layer Heat Transfer*, AIAA-72-717, June, 1972.

[7] D. E. Nestler, *The Effects of Surface Discontinuities on Convective Heat Transfer in Hypersonic Flow*, AIAA-85-0971, June, 1985.

[8] D. E. Nestler, A. R. Saydah, and W. L. Auxer, *Heat Transfer to Steps and Cavities in Hypersonic Turbulent Flow*, AIAA-68-673, June, 1968.

[9] D. H. Richbourg, *A Three-Dimensional Boundary-Layer Computer Program for Sphere-Cone Type Reentry Vehicles*, Volume 2, User's Manual, AFFDL-TR-78-67, June, 1978.

[10] A. L. Thornton, *LOVEL-84: A Low Velocity Aerodynamic Heating Code for Flat Plates, Wedges, and Cones*, SAND84-0457, Sandia National Laboratories, Albuquerque, May, 1984.

[11] I. Weinstein, D. E. Avery, and A. J. Chapman, *Aerodynamic Heating to the Gaps and Surfaces of Simulated Reusable-Surface-Insulation Tile Arrays in Turbulent Flow at Mach 6.6*, NASA TM X-3225, November, 1975.

Appendix A
Vehicle Trajectory

Computed Atmospheric Trajectory

	TIME	EL ANG DEG	ALT (Z) FT	VEL(E) FPS	RANGE FT	MACH	ACC(L) FPS/S	THRUST G	DRAG G	Q PSF	RN/L 1/FT	INST. WT LB
F	0.00	32.500	35.0	0.0	0.0	0.00	-17.3	.001	0.000	0.000	0.000	2761.500
FM	.07	32.500	35.0	0.0	0.0	0.00	.0	.537	0.000	0.000	0.000	2761.227
	.20	32.500	35.7	35.2	1.0	.03	516.2	16.581	-.000	1.474	224680.778	2744.298
L	.40	32.500	44.9	138.6	15.5	.12	525.5	16.874	-.004	22.809	883789.687	2696.614
	.40	32.483	45.0	139.4	15.7	.12	525.6	16.877	-.004	23.075	888927.013	2696.246
	.60	30.807	65.1	245.6	48.5	.22	536.0	17.184	-.012	71.568	1565027.529	2648.193
	.80	29.732	95.2	353.8	100.3	.32	546.4	17.502	-.024	148.434	2252889.652	2600.141
	1.00	28.941	135.3	464.1	171.6	.42	556.9	17.833	-.042	255.139	2951979.700	2552.089
	1.20	28.317	185.1	576.6	262.9	.52	567.5	18.177	-.065	393.159	3661884.021	2504.036
	1.40	27.802	244.7	691.1	374.8	.62	578.3	18.535	-.094	563.981	4382252.647	2455.984
	1.60	27.365	314.0	807.9	507.6	.72	589.0	18.908	-.140	769.045	5112555.436	2407.932
	1.80	26.986	393.2	926.8	661.9	.83	599.4	19.296	-.213	1009.709	5852148.837	2359.879
	2.00	26.653	482.2	1047.5	838.1	.94	607.7	19.701	-.363	1286.593	6598665.469	2311.827
	2.20	26.355	581.2	1169.2	1036.5	1.05	602.5	20.123	-.953	1598.516	7346531.112	2263.775
	2.40	26.085	689.8	1290.1	1257.1	1.15	607.3	20.564	-1.248	1939.751	8082824.842	2215.722
	2.60	25.840	808.1	1412.1	1500.0	1.26	613.7	21.026	-1.517	2316.168	8821203.318	2167.670
	2.80	25.614	936.0	1535.5	1765.6	1.38	620.6	21.509	-1.789	2728.487	9562057.261	2119.618
	3.00	25.406	1073.6	1660.7	2054.0	1.49	627.4	22.015	-2.085	3178.523	10307534.321	2071.565
	3.20	25.212	1220.2	1758.2	2363.9	1.58	345.3	13.488	-2.329	3547.161	10875550.744	2033.124
	3.40	25.024	1371.6	1799.5	2686.9	1.61	66.1	4.588	-2.110	3699.312	11093777.246	2013.903
BO	3.50	24.932	1447.6	1798.8	2850.1	1.61	-78.9	.074	-2.106	3687.901	11070916.401	2011.500
NP	3.50	24.932	1447.6	1798.8	2850.1	1.61	-103.2	0.000	-2.785	3687.901	11070916.401	1393.000
	3.60	24.838	1523.1	1788.5	3012.8	1.61	-101.9	0.000	-2.747	3637.773	10990128.734	1393.000
	3.80	24.650	1671.9	1766.6	3335.7	1.59	-112.9	0.000	-3.093	3533.197	10821800.305	1393.000
	4.00	24.459	1817.8	1744.3	3655.0	1.57	-110.3	0.000	-3.013	3429.397	10654111.500	1393.000
	4.20	24.265	1960.8	1722.5	3970.8	1.55	-107.7	0.000	-2.937	3329.803	10492269.381	1393.000
	4.40	24.069	2100.9	1701.2	4283.2	1.53	-105.2	0.000	-2.863	3234.442	10331346.043	1393.000
	4.60	23.870	2238.3	1680.4	4592.1	1.51	-102.8	0.000	-2.792	3143.008	10172820.446	1393.000
	4.80	23.668	2373.0	1660.0	4897.8	1.50	-100.5	0.000	-2.724	3055.220	10018167.971	1393.000
	5.00	23.463	2504.9	1640.1	5200.3	1.48	-98.3	0.000	-2.658	2970.896	9867276.874	1393.000
	5.50	22.939	2823.2	1592.3	5943.0	1.44	-93.0	0.000	-2.502	2774.134	9505806.207	1393.000
	6.00	22.397	3125.7	1547.0	6667.1	1.40	-88.2	0.000	-2.360	2595.302	9166766.430	1393.000
	6.50	21.837	3412.9	1504.1	7373.6	1.36	-83.6	0.000	-2.228	2432.123	8849883.496	1393.000
	7.00	21.260	3685.4	1463.3	8063.5	1.33	-79.4	0.000	-2.106	2283.166	8552297.963	1393.000
	7.50	20.664	3943.6	1424.6	8737.6	1.29	-75.5	0.000	-1.993	2146.934	8272545.388	1393.000
	8.00	20.049	4188.2	1387.8	9396.8	1.26	-71.8	0.000	-1.889	2022.329	8010122.792	1393.000
	8.50	19.416	4419.6	1352.8	10041.6	1.23	-68.4	0.000	-1.793	1908.090	7763489.282	1393.000
	9.00	18.764	4638.1	1319.4	10672.8	1.20	-65.1	0.000	-1.703	1803.124	7531270.995	1393.000
	9.50	18.094	4844.1	1287.7	11291.1	1.17	-61.6	0.000	-1.605	1706.895	7313227.057	1393.000
	10.00	17.404	5038.1	1257.7	11897.1	1.14	-58.4	0.000	-1.515	1618.799	7108907.796	1393.000
	10.50	16.696	5220.5	1229.3	12491.5	1.12	-55.3	0.000	-1.433	1537.969	6917200.651	1393.000
	11.00	15.969	5391.4	1202.4	13074.8	1.10	-52.5	0.000	-1.358	1463.653	6737107.442	1393.000
	11.50	15.223	5551.3	1176.7	13647.6	1.07	-49.9	0.000	-1.290	1395.200	6567750.347	1393.000
	12.00	14.458	5700.5	1152.4	14210.4	1.05	-47.5	0.000	-1.227	1332.058	6408387.014	1393.000
	12.50	13.675	5839.2	1130.7	14763.9	1.03	-39.1	0.000	-.979	1277.076	6266539.256	1393.000
	13.00	12.876	5968.0	1113.0	15309.7	1.02	-32.2	0.000	-.777	1232.501	6148744.331	1393.000
	13.50	12.062	6087.3	1098.3	15849.3	1.00	-26.7	0.000	-.620	1195.904	6049905.515	1393.000

	TIME	EL ANG DEG	ALT (Z) FT	VEL(E) FPS	RANGE FT	MACH	ACC(L) FPS/S	THRUST G	DRAG G	Q PSF	RN/L 1/FT	INST. WT LB
	14.00	11.236	6197.6	1085.8	16384.1	.99	-24.3	0.000	-.561	1164.751	5964305.416	1393.000
	14.50	10.398	6298.9	1073.9	16914.4	.98	-23.0	0.000	-.535	1135.986	5884491.590	1393.000
	15.00	9.548	6391.5	1062.7	17440.4	.97	-21.8	0.000	-.513	1109.248	5809673.402	1393.000
	15.50	8.688	6475.2	1052.1	17962.4	.96	-20.7	0.000	-.491	1084.400	5739618.185	1393.000
	16.00	7.818	6550.4	1042.0	18480.5	.95	-19.6	0.000	-.472	1061.322	5674115.069	1393.000
	16.50	6.937	6617.0	1032.5	18994.8	.95	-18.5	0.000	-.454	1039.904	5612972.508	1393.000
	17.00	6.047	6675.1	1023.5	19505.5	.94	-17.5	0.000	-.438	1020.048	5556016.127	1393.000
	17.50	5.147	6724.9	1015.0	20012.7	.93	-16.5	0.000	-.423	1001.665	5503086.842	1393.000
	18.00	4.239	6766.2	1007.0	20516.5	.92	-15.5	0.000	-.409	984.675	5454039.214	1393.000
	18.50	3.323	6799.3	999.5	21017.0	.92	-14.6	0.000	-.396	969.005	5408740.004	1393.000
	19.00	2.399	6824.2	992.4	21514.3	.91	-13.7	0.000	-.385	954.589	5367066.890	1393.000
	19.50	1.468	6840.9	985.8	22008.6	.90	-12.9	0.000	-.374	941.367	5328907.338	1393.000
	20.00	.531	6849.5	979.6	22499.8	.90	-12.0	0.000	-.364	929.284	5294157.600	1393.000
AP	20.28	.000	6850.7	976.2	22775.5	.89	-11.6	0.000	-.359	922.953	5276028.622	1393.000
	20.50	-.412	6850.0	973.7	22988.1	.89	-11.2	0.000	-.355	918.290	5262721.820	1393.000
	21.00	-1.360	6842.5	968.3	23473.5	.89	-10.4	0.000	-.347	908.340	5234511.123	1393.000
	21.50	-2.314	6827.0	963.3	23956.2	.88	-9.6	0.000	-.340	899.391	5209443.301	1393.000
	22.00	-3.271	6803.6	958.7	24436.1	.88	-8.9	0.000	-.333	891.407	5187441.577	1393.000
	22.50	-4.232	6772.3	954.4	24913.3	.87	-8.2	0.000	-.327	884.353	5168434.424	1393.000
	23.00	-5.196	6733.2	950.5	25388.0	.87	-7.4	0.000	-.322	878.195	5152354.937	1393.000
	23.50	-6.162	6686.2	947.0	25860.0	.87	-6.8	0.000	-.317	872.906	5139140.362	1393.000
	24.00	-7.130	6631.5	943.8	26329.5	.86	-6.1	0.000	-.313	868.458	5128731.670	1393.000
	24.50	-8.099	6569.1	940.9	26796.5	.86	-5.4	0.000	-.309	864.826	5121073.166	1393.000
	25.00	-9.068	6499.0	938.4	27261.0	.86	-4.8	0.000	-.306	861.989	5116112.138	1393.000
	25.50	-10.037	6421.2	936.1	27723.1	.86	-4.2	0.000	-.304	859.925	5113798.534	1393.000
	26.00	-11.006	6335.9	934.2	28182.8	.85	-3.6	0.000	-.302	858.614	5114084.671	1393.000
	26.50	-11.973	6242.9	932.5	28640.1	.85	-3.0	0.000	-.300	858.040	5116924.969	1393.000
EP	26.72	-12.394	6200.0	931.9	28838.9	.85	-2.7	0.000	-.300	858.016	5118952.532	1393.000
F	26.72	-12.394	6200.0	931.9	28838.9	.85	5.5	.230	-.272	858.016	5118952.532	1393.000
	27.00	-12.887	6136.2	1149.7	29123.1	1.05	811.3	26.120	-1.128	1308.331	6324948.789	1352.084
	27.50	-13.554	5981.0	1559.5	29782.0	1.42	828.6	27.693	-2.173	2418.845	8612789.934	1275.029
	28.00	-14.062	5769.6	1981.1	30640.8	1.81	855.4	29.466	-3.122	3928.508	10998114.241	1197.974
	28.50	-14.470	5498.8	2405.8	31704.6	2.19	818.6	30.111	-4.917	5840.867	13444740.444	1121.526
	29.00	-14.821	5176.8	2600.1	32936.2	2.37	-64.4	3.744	-6.001	6889.224	14646066.516	1079.829
	29.50	-15.166	4844.0	2544.3	34179.2	2.31	-120.0	1.844	-5.836	6663.225	14449358.854	1075.195
	30.00	-15.520	4511.4	2483.1	35391.4	2.26	-124.6	1.501	-5.640	6410.924	14218003.787	1071.785
	30.50	-15.882	4179.7	2419.7	36571.4	2.20	-128.8	1.155	-5.431	6149.488	13969085.903	1069.162
	31.00	-16.253	3849.4	2354.4	37718.4	2.13	-132.6	.807	-5.209	5880.695	13703803.850	1067.325
	31.50	-16.633	3521.0	2287.2	38831.4	2.07	-136.2	.457	-4.977	5605.491	13421612.397	1066.275
BO	31.92	-16.960	3248.1	2229.6	39735.4	2.02	-139.0	.164	-4.776	5371.072	13172024.595	1066.000
NP	31.92	-16.960	3248.1	2229.6	39735.4	2.02	-46.8	0.000	-1.745	5371.072	13172024.595	800.000
	32.00	-17.025	3194.8	2225.8	39909.9	2.01	-46.7	0.000	-1.744	5361.233	13166569.321	800.000
	32.50	-17.422	2867.0	2202.5	40967.4	1.99	-46.4	0.000	-1.742	5301.001	13134446.342	800.000
	33.00	-17.823	2535.4	2179.3	42011.5	1.97	-46.3	0.000	-1.745	5240.722	13101696.050	800.000
	33.50	-18.227	2200.0	2156.2	43042.2	1.94	-46.2	0.000	-1.748	5181.127	13065304.390	800.000
	34.00	-18.635	1860.9	2133.2	44059.5	1.92	-46.1	0.000	-1.751	5122.569	13018825.675	800.000
	34.50	-19.046	1518.4	2110.2	45063.5	1.89	-46.0	0.000	-1.754	5064.543	12967841.391	800.000
	35.00	-19.461	1172.4	2087.2	46054.2	1.87	-45.8	0.000	-1.756	5006.287	12925162.595	800.000
	35.50	-19.879	823.0	2064.4	47031.5	1.85	-45.6	0.000	-1.757	4947.910	12891011.322	800.000
	36.00	-20.300	470.4	2041.7	47995.6	1.83	-45.3	0.000	-1.756	4889.517	12865636.050	800.000
	36.50	-20.726	114.7	2019.1	48946.4	1.81	-45.0	0.000	-1.753	4831.210	12849315.232	800.000
GR EP	36.66	-20.863	.0	2011.9	49248.5	1.80	-44.9	0.000	-1.752	4812.547	12846049.035	800.000

Trajectory After Water Entry

Time (sec)	Velocity (ft/sec)	Depth (ft)	Temperature (deg R)
0.0000E+00	0.2012E+04	0.0000E+00	0.5417E+03
0.1000E+00	0.1405E+04	0.6000E+02	0.5410E+03
0.2000E+00	0.1100E+04	0.1060E+03	0.5404E+03
0.3000E+00	0.8850E+03	0.1390E+03	0.5397E+03
0.4000E+00	0.7100E+03	0.1680E+03	0.5391E+03
0.5000E+00	0.5700E+03	0.1890E+03	0.5387E+03
0.6000E+00	0.4600E+03	0.2070E+03	0.5383E+03
0.7000E+00	0.3600E+03	0.2230E+03	0.5380E+03
0.8000E+00	0.2700E+03	0.2340E+03	0.5377E+03
0.9000E+00	0.1850E+03	0.2380E+03	0.5376E+03
0.1000E+01	0.1050E+03	0.2430E+03	0.5375E+03
0.1200E+01	0.8500E+02	0.2520E+03	0.5373E+03
0.1400E+01	0.6500E+02	0.2610E+03	0.5371E+03
0.1600E+01	0.5250E+02	0.2700E+03	0.5369E+03
0.1800E+01	0.4750E+02	0.2790E+03	0.5367E+03
0.2000E+01	0.4600E+02	0.2880E+03	0.5365E+03
0.4000E+01	0.4600E+02	0.3770E+03	0.5340E+03
0.6000E+01	0.4600E+02	0.4660E+03	0.5314E+03
0.8000E+01	0.4500E+02	0.5540E+03	0.5285E+03
0.1000E+02	0.4400E+02	0.6430E+03	0.5256E+03
0.1200E+02	0.4400E+02	0.7320E+03	0.5225E+03

Appendix B

Gap Heating Data Derived From Reference 11

Run	δ^* (cm)	L (cm)	H (cm)	$\left[\frac{q}{q_{FP}}\right]_D$	$\left[\frac{q}{q_{FP}}\right]_U$	$\left[\frac{q}{q_{FP}}\right]_{avg}$
8	0.81	0.18	0.353	0.500	0.199	0.350
			0.510	0.292	0.160	0.226
			0.625	0.172	0.116	0.144
			0.750	0.097	0.094	0.096
6	1.17	0.18	0.510	0.171	0.115	0.143
			0.625	0.113	0.085	0.099
			0.750	0.066	0.063	0.065
5	1.17	0.30	0.510	0.276	0.275	0.275
			0.625	0.185	0.238	0.212
			0.750	0.111	0.212	0.162
			0.850	0.052	0.206	0.129
4	1.17	0.41	0.510	0.312	0.263	0.288
			0.625	0.229	0.222	0.226
			0.750	0.137	0.196	0.167
			1.162	0.000	0.153	0.077
7	1.62	0.18	0.510	0.148	0.064	0.106
			0.625	0.093	0.040	0.067
			0.706	0.061	0.028	0.045
			0.750	0.048	0.022	0.035

where

$D =$ quantity measured on the downstream cavity wall

$U =$ quantity measured on the upstream cavity wall

$avg =$ average of the upstream and downstream wall values

Distribution

1510 J. W. Nunziato
1520 D. J. McCloskey
1530 L. W. Davison
1540 R. C. Luth
1550 R. C. Maydew
1551 J. K. Cole
1552 C. W. Peterson
1553 S. McAlees, Jr.
1553 D. N. Benton (5)
1554 D. D. McBride
1555 W. R. Barton
1556 W. L. Oberkampf
3141 S. A. Landenberger (5)
3151 W. L. Garner
8024 P. W. Dean
8150 J. B. Wright
8152 J. C. Swearengen
8152 M. T. Ferrario

```
TTTTTTT    6666666666666  E     N  NN  D   D          O   O  F           F
                          E     N   N  D   D          O   O  F           F
                          EEEEE  N   N  DDDD           OOO   F           F

                                        DDDD   N   N  BBBB   EEEEE  N   N  TTTTT
                                        D   D  N   N  B   B  E      N   N    T
                                        D   D  NN  N  B   B  E      NN  N    T
                                        D   D  N N N  BBBB   EEEE   N N N    T
                                        D   D  N  NN  B   B  E      N  NN    T
                                        D   D  N   N  B   B  E      N   N    T
                                        DDDD   N   N  BBBB   EEEEE  N   N    T

                                  AAA    SSSS  PPPP          BBBB    III   TTTTT
                                 A   A  S      P   P         B   B    I      T
                                 A   A  S      P   P         B   B    I      T
                                 A   A   SSS   PPPP          BBBB     I      T
                                 AAAAA      S  P             B   B    I      T
                                 A   A      S  P             B   B    I      T
                                 A   A  SSSS   P          ..  BBBB    III     T
```

lifiers: /NOFEED /FLAG /FORM=DEFAULT /LENGTH=66 /LIBRARY=SYS$SYSROOT:[SYSLIB]TALD
/TRUNCATE /WIDTH=132

e 7DUA3:[DNBENTO.ASP.PRESS]ASP.BIT;1 (5287,9,0), last revised on 4-MAR-1987 0
[176,1]. The records are variable length with implied (CR) carriage control. T

BOX.034 (1572) queued to SAV07_LCB0 on 4-MAR-1987 08:52 by user DNBENTO, UIC [17
pleted on printer _SAV07$LCB0: on 4-MAR-1987 08:52 from queue SAV07_LCB0.

```
TTTTTTT    66666666666666666666666666666666666666666666666666666666666666666666
TTTTTTT    66666666666666666666666  Digital Equipment Corporation - VAX/VMS Vers
TTTTTTT    66666666666666666666666666666666666666666666666666666666666666666666

      1         2         3         4         5         6         7         8
45678901234567890123456789012345678901234567890123456789012345678901234567890123
```